参赛队员姓名： 王径源

中学： 包玉刚实验学校

省份： 上海市

国家/地区： 中国

指导教师姓名： Xuan Luo

指导教师单位： National Graphene Research and Development Research (US)

论文题目: Theoretical investigation of the BCN monolayers and its derivatives for metal-free CO2 photocatalysis, capture, and utilization

Theoretical investigation of the boron-nitride-carbon monolayer and their derivatives for metal-free CO_2 photocatalysis, capture, and utilization

Jingyuan Wang

Abstract

In recent years, carbon capture and utilization (CCU) has been an attractive solution to global warming, mainly caused by increasing CO_2 emission levels. Many functional materials have been developed for removing atmospheric CO_2 and converting it into more useful forms. Due to traditional metallic species' drawbacks of photo-corrosion, poor visible light absorbance, and environmental damages, metal-free materials attracted research interest. In particular, boron nitride (BN) possesses unique B–N channels with high electronegativity difference, which facilitates CO_2 reduction, and boron-carbon-nitride (BCN) has demonstrated CO_2 reduction catalytic abilities under visible light, which makes them prospective materials for photocatalysis. However, further modification of the materials and their applicability in other CCU purposes has not been extensively explored. Therefore, we aim to investigate ways to modify BCN monolayers so their properties can primarily better suit the requirement of CO_2 photocatalysts along with those of carbon capture materials or other optoelectronic materials. In this research, we modified various BCN monolayers with metal-free substitutional doping and nitrogen vacancies and performed first-principles calculations based on density functional theory. The effects on band gap tuning, charge transfer, and CO_2 adsorption ability are studied. Specifically, O_N-$B_{13}C_8N_{11}$ and Si_C-2×2-BC_6N show suitable CO_2 reduction photocatalysts properties, and O_C-2×2-BC_6N and N_v-4×4-BN can be considered for future CO_2 capture materials. The results contribute to existing CCU approaches, highlight the potential of BCN monolayer modifications that are worth further investigation, and offer insights for other photocatalyst applications.

Keywords: Photocatalysis, CO_2 conversion, carbon capture and utilization, density functional theory, boron-nitride-carbon

Introduction

Global warming affects multiple aspects of the environment and threatens human health. The average global temperature in 2022 was 1.15 °C above that in 1850–1900.[1] The increase in global temperature has led to the melting of ice caps, rise in sea levels, loss of coastal land, reductions in biodiversity, and increased risk of extreme weather conditions.[2] According to the World Health Organization, climate change is expected to cause approximately 250,000 additional deaths annually after 2030.[3] Despite global efforts to address this impending crisis, fossil fuels remain the primary source of energy, highlighting the urgent need to control the levels of produced atmospheric carbon dioxide.[4,5] Scientists have made many attempts to respond to the increasing CO_2 level problem. Existing approaches can be generally categorized as either carbon capture and storage (CCS) approaches or carbon capture and utilization (CCU) approaches.[6] Both approaches include the selective removal of CO_2 gas from the atmosphere. Current carbon capture routes include absorption-based methods, membrane separation, adsorption-based methods, chemical looping, and direct air capture in post-combustion, pre-combustion, or with the use of oxyfuel combustion. In CCS, after CO_2 is captured, it is compressed and sequestered in geological formations.[7] However, the high cost and uncertain long-term effects of CCS make the CCU strategy a more attractive and feasible alternative.[6] CCU aims to transform the captured CO_2 into other valuable products, such as carboxylic acids, alcohols, aldehydes, etc., or to use the gas to replace conventional raw materials in industrial processes.[8] Various materials that can adsorb CO_2 and catalyze the most crucial step in this approach, that is, the CO_2 reduction reaction (CRR), with high selectivity and efficiency have been investigated.[4,9] Methods such as CO_2 electrocatalysis, photocatalysis, and CO_2 biotransformation have demonstrated promise for transforming greenhouse gases into value-added compounds or photoelectric materials.[10,11]

Among these methods, the photocatalyzed CRR stands out because it can utilize sunlight, a widely available and sustainable energy source, to produce the CUU products.[4,10] In photocatalyzed CRR, photons are absorbed by the photocatalyst to create electrons that participate in the reduction reaction of adsorbed CO_2, and the final products will be desorbed from the material.[12] Chemisorption is a necessary condition required to transfer electrons from the photocatalyst to the adsorbed gas and activate it.[13] Recent research focusing on finding suitable photocatalysts and understanding the CRR mechanism indicates that photocatalytic CRR is one of the most effective methods for managing CO_2 levels. Thus, there is a need for further studies in this field.[14]

Many materials have been developed to adsorb CO_2 and act as a photocatalyst, thereby enabling the chemically inert gas to undergo chemical reactions.[15–17] Since Geim et al. successfully isolated the monolayer graphene in 2004 and won the Nobel Prize in Physics in 2010 for this discovery, two-dimensional (2D) materials have been widely researched both theoretically and experimentally, including their usage as CRR photocatalysts.[18] 2D materials exhibit remarkable chemical and physical properties, including a large surface area, which provides accessible active sites, thinness, which minimizes the migration distance of photogenerated carriers, and a 2D planar structure, which facilitates material modification to further improve their properties.[18] These properties align with the requirements of CRR photocatalysts well. Existing CRR 2D photocatalysts include metal-containing catalysts, such as metal oxides, metal sulfides, bismuth oxyhalides, MXenes, 2D metal-organic frameworks, and metal-free catalysts, such as graphene and its derivatives, carbon nitride, and boron nitride (BN) monolayers.[4,19–23] Although the catalytic performance of metal-free 2D photocatalysts is not as good as that of metal-containing 2D photocatalysts in terms of their production rate, metallic species are prone to photo-corrosion and have poor absorption of visible light. Moreover, because metal-free monolayer materials use lightweight and abundant elements, which aligns with the concept of green chemistry, research interest has shifted toward improving metal-free photocatalysts through surface modification.[4,24] For example, graphene and its derivatives exhibit tunable band gaps and enhanced catalytic activity by doping with heteroatoms (O, B, N, P, etc.).[25] Therefore, metal-free monolayer photocatalysts are particular interesting and worthy of a detailed investigation.

BN monolayers have a structure similar to that of graphene and possess a wide indirect band gap, which is unsuitable for photocatalysis. [26] However, BN has a unique B–N channel characterized by a high electronegativity difference that promotes the photoreduction reaction.[13] Thus, to take advantage of this high electronegativity difference, modifications are needed to address the large indirect band gap (approximately 5.5 eV) and weak CO_2 adsorption due to unreactive surface chemistry.[4,13] When BN is doped with O, N, or P, its visible-light absorption and photoactivity are enhanced.[13] Doping BN with Fe or Ni dimers and CuMn heteronuclear dimers leads to improved CO_2 to CH_4 conversion.[27] When doped with C, h-BCN nanosheets can catalyze the H_2 and O_2 evolution reactions.[28] Doping the lattice structure with aromatic carbon induces visible-light absorption and catalysis.[26] Novel BCN monolayers may exhibit a diverse set of analogous material properties by tuning the B, C, and N atomic arrangements and concentrations.[26] Given the variable

properties of such materials, BCN monolayers have been used in a wide range of applications, including gas sensors, catalysis, and energy storage.[28]

Many BCN studies prioritized photocatalytic water splitting and other applications over developing and characterizing CO_2 reduction photocatalysis.[28] However, some researchers found that BCN monolayers showed a greater ability to absorb CO_2 than graphene.[29] Other groups calculated CO_2 adsorption energies (E_{ad}) on BC_6N and BC_3N_2 monolayers, both showing weak interactions.[30,31] Previous studies also experimentally confirmed that BCN can reduce CO_2 to CO under visible-light illumination.[26] However, metal-free modifications of BCN for photocatalysis are not well understood.

We aim to investigate new BCN monolayer structures suitable for CO_2 reduction photocatalyst while other CCU applications are considered. Various 2D BCN configurations have been proposed and can be grouped based on their B to N molar ratio, which changes their electronic structure and material properties. Here, we investigated $B_{13}C_8N_{11}$ and $B_{11}C_{12}N_9$ as representative BCN structures with more B atoms than N atoms. BC_6N as a structure with equal numbers of B and N atoms, and $B_{11}C_8N_{13}$ and $B_9C_{12}N_{11}$ as structures with more N atoms than B atoms. These structures were chosen and proposed based on relevant structures reported in prior studies.[26,30] Oxygen substitutional doping was conducted to achieve the metal-free modification of the materials. Because O-doping on the BN monolayer induces chemisorption, a similar effect is expected to occur on the BCN monolayers.[32] The target band gap of an ideal photocatalyst that absorbs visible light is in the range of 1.8–2.5 eV.[13] Moreover, the target E_{ad} for chemisorption is ≥ 0.3 eV.[33] We used density functional theory (DFT) to calculate the most stable atomic structures of the BN, BC_6N, $B_{13}C_8N_{11}$, $B_{11}C_{12}N_9$, $B_{11}C_8N_{13}$, and $B_9C_{12}N_{11}$ monolayers as well as C-doped, O-doped, Si-doped, and N-vacancy-modified monolayers. We then calculated the binding energies of CO_2 on these monolayer surfaces to determine whether chemisorption is possible. Band structures and charge transfers were also calculated to determine the monolayer with the best potential for use as a CO_2 reduction photocatalysis and other capture and utilization applications. As such, this novel research contributes to further development of new and existing CCU approaches.

Experimental

A suitable band gap for visible-light absorption (i.e., in the range of 1.8–2.5 eV) and sufficient chemisorption of CO_2 (i.e., E_{ad} ≥ 0.3 eV) are the two main parameters used to assess potential CO_2

photocatalysts, which is the primary aim of this research.[13,33] Hereafter, substitutional doping is denoted as X_Y, where X represents the dopant and Y is the substituted atom. Nitrogen vacancies are denoted as N_v.

Computational details

We performed first-principles calculations based on DFT within the Perdew–Burke–-Ernzerhof (PBE) generalized gradient approximation (GGA) implemented in the ABINIT code.[34] The projected augmented wave (PAW) method was used to generate pseudopotentials with the ATOMPAW code.[35,36] The electron configurations and radius cutoffs used for B, C, N, O, and Si were $[He]2s^2 2p^1$ and 0.90 Å, $[He]2s^2 2p^2$ and 0.79 Å, $[He]2s^2 2p^3$ and 0.64 Å, $[He]2s^2 2p^4$ and 0.74 Å, and $[Ne]3s^2 3p^2$ and 1.01 Å, respectively.

In all calculations, the self-consistent field (SCF) was terminated when the total energy difference was smaller than 2.7×10^{-9} eV twice consecutively. The converged values for the kinetic energy cutoff, vacuum height of the unit cells, and Monkhorst–Pack *k*-point grids were considered to be reached when the total energy difference was smaller than 2.7×10^{-3} eV twice consecutively.

The Broyden–Fletcher–Goldfarb–Shanno (BFGS) minimization algorithm was used in the structural optimization calculations. The maximum force tolerance used was 2.6×10^{-3} eV/Å (5.0×10^{-5} Ha/Bohr).

Atomic structures

Convergence calculations for the vacuum height, kinetic energy cutoff, and *k*-mesh were conducted using the abovementioned criteria before the structural optimization calculations. To converge the cell size and relax the bond length of CO_2, we used the molecule-in-a-big-box method. For all pure and modified monolayers, from the primitive cell to all 4×4 cell shown in Table 1, the slab model was used. The vacuum height, kinetic energy cutoff, and *k*-mesh were converged according to the abovementioned criterion.

The modified monolayers used the same vacuum height, energy cutoff (i.e., the highest value obtained), and *k*-mesh as the 4×4-BN and 2×2-BC_6N monolayers. All structures were relaxed using these values via the BFGS method to obtain the optimized coordinates of the atoms. The relaxed coordinates were used to calculate the electronic structures and total energies of all monolayers.

For the CO_2 monolayer complexes, we placed CO_2 in the middle of the bridge site between the B–C bond parallel to the plane in the pristine BCN structures. In the O- and Si-doped BCN structures, CO_2 was placed vertically in the hexagonal centers. In N_v-4×4-BN, CO_2 was inserted vertically into a vacant hole. Full relaxations of the complex interfaces were conducted to obtain the optimized structures and lattice parameters used for the electronic structure and total energy calculations.

Adsorption Energy

The adsorption energy (E_{ad}) between CO_2 and the monolayer is needed to assess whether the molecule is chemisorbed or physisorbed on the monolayer surface and whether the reduction reaction can occur. Thus, E_{ad} is crucial for determining the effectiveness of a photocatalyst. E_{ad} can be found with the following equation:

$$E_{ad} = E_{CO_2+ML} - E_{ML} - E_{CO_2} \qquad (1)$$

where E_{CO_2+ML} is the total energy of the complex interface, E_{ML} is the total energy of the monolayers, and E_{CO_2} is the total energy of CO_2. A negative E_{ad} indicates that CO_2 is adsorbed on the monolayer, and the more negative the value of E_{ad}, the stronger the adsorption. When $E_{ad} \leq -0.3$ eV, chemisorption occurs.

Electronic structures

Band structure. The band structures of the monolayers and complexes formed after CO_2 adsorption were calculated. The high-symmetry *k*-point circuit was *M* (½,0,0), Γ (0,0,0), *K* (⅓,⅔,0), and *M* (½,0,0), as shown in Fig. 1. The direct band gap is preferred for efficient photocatalysis.

Charge transfer. Monolayers that demonstrated CO_2 chemisorption were selected for the charge-transfer calculations. The charge transfer that occurred is indicated by a difference in charge density between the isolated monolayer and CO_2 and the combined complex and is calculated as follows:

$$\Delta\rho(r) = \rho_{CO_2+ML}(r) - \rho_{ML}(r) - \rho_{CO_2}(r) \qquad (2)$$

where ρ_{CO_2+ML} (r), ρ_{ML} (r), and ρ_{CO_2} (r) represent the charge densities of the monolayer and CO_2 complex, monolayer, and CO_2, respectively.

Results and discussion

To study whether the monolayers can serve as a photocatalyst or applied for other purposes, we calculated the atomic and electronic structures, E_{ad}, and charge transfer of CO_2 adsorbed on the pure and modified monolayers.

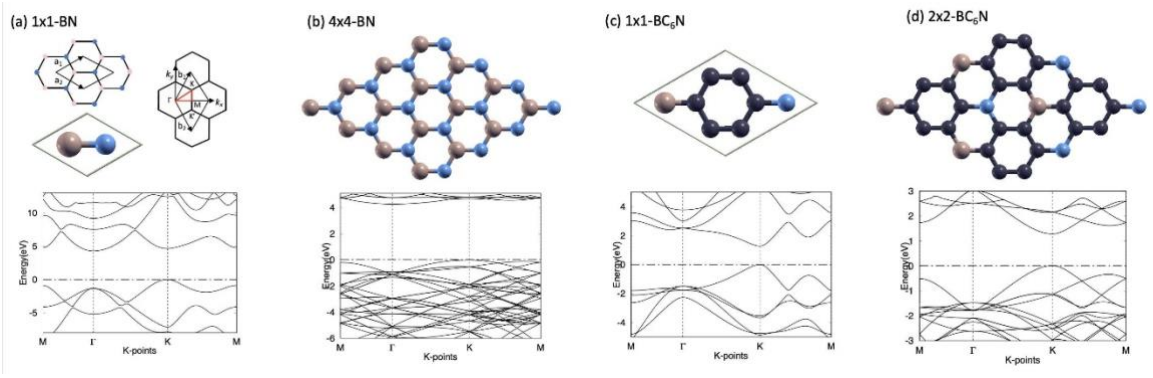

Fig. 1. (a) Real and reciprocal space lattice vectors of the BN monolayers. The high-symmetry *k*-points in the first Brillouin zone are *M* (½,0,0), Γ (0,0,0), *K* (⅓,⅔,0), and *M* (½,0,0), and the *k*-point circuit is shown in red. The primitive cell and band structure plot of the BN monolayer are also shown. (b) 4×4-BN monolayer atomic structure and band structure plot. (c) BC_6N primitive cell and band structure plot. (d) 2×2-BC_6N atomic structure and band structure plot. The Fermi level was set to 0 eV. B, C, and N atoms are shown in pink, black, and blue, respectively.

Table 1. Calculated lattice parameters *a* (Å) for the fully optimized monolayers used in this study.

Monolayer	*a* (Å)
4×4-BN	10.05
N_v-4×4-BN	9.95
C_2-doped-4×4-BN	10.05
C_4-doped-4×4-BN	10.04
$B_{13}C_8N_{11}$	10.12
O_C-$B_{13}C_8N_{11}$	10.08
O_N-$B_{13}C_8N_{11}$	10.10
$N_{13}C_8B_{11}$	9.96
$B_{11}C_{12}N_9$	10.53
$N_{11}C_{12}B_9$	9.94
2×2-BC_6N	9.96
O_C-2×2-BC_6N	9.94
O_N-2×2-BC_6N	9.98
Si_C-2×2-BC_6N	10.13

Pure monolayers calculations

We first calculated the relaxed structures of CO_2, BN primitive cell, and BC_6N primitive cell that are consistent with previous studies and the values were used in later calculations. The CO_2 molecule was relaxed to a linear structure and to a bond length of 1.17 Å, which agrees well with previous theoretical and experimental values of 1.16 Å.[37,38] The BN monolayer has a two-atom primitive cell and a large indirect band gap, as shown in Fig. 1(a). The length of the lattice parameter after relaxation is 2.51 Å, which is consistent with a previous theoretical of 2.49 Å and an experimentally obtained value of 2.54 Å.[26,39] The BC_6N primitive cell, as shown in Fig. 1(c), was relaxed to a lattice parameter of 4.98 Å, which is consistent with the previous theoretical value (5.01 Å).[30] The primitive cells were used for the 4x4 cells shown in Fig. 1(b) and 1(d).

Atomic and electronic structures of the monolayers

Using the values obtained from pure monolayers calculations, the optimized atomic structures of the modified monolayers were obtained after full relaxation. The lattice parameters of all monolayers are listed in Table 1, and their atomic and corresponding band structures are shown in Fig. 2.

After relaxation, both $N_{11}C_{12}B_9$ and O_C-2×2-BC_6N have the smallest lattice constant, at9.94 Å. As the atomic radii of N and

O atoms are smaller than those of B and other atoms present, higher concentrations of N and O and a low concentration of B contribute to the decrease in lattice size. Moreover, the largest monolayer is $B_{11}C_{12}N_9$, with a lattice constant of 10.53 Å, which is even greater than that of Si_C-2×2-BC_6N (10.13 Å). This expansion in lattice size can be attributed to the high B concentration and low N concentration of the monolayer. As B atoms have a relatively large atomic radius, a structure predominantly formed with B tend to be larger.

Additionally, as shown in Table 1, BC_6N and its derivatives tend to have smaller lattice parameters than the other studied monolayers. This is because the average C–C bond length of approximately 1.39 Å is longer than the B–N bond length of approximately 1.44–1.45 Å. Therefore, a high concentration of C–C pairs results in a smaller lattice parameter.

The results in Table 2 and Fig. 2 show the various types of band structures observed for the studied monolayers. The structures we are most interested in are those with a direct band gap in the range of 0.875–2.55 eV after adjusting for the DFT calculation underestimations, i.e., those capable of visible-light absorption. Therefore, only O_N-$B_{13}C_8N_{11}$ (2.44 eV), 2×2-BC_6N (1.27 eV), and Si_C-2×2-BC_6N (0.90 eV) are suitable for CO_2 photocatalysis. Moreover, for $B_{13}C_8N_{11}$, $N_{13}C_8B_{11}$, $B_{11}C_{12}N_9$, and $N_{11}C_{12}B_9$, which have similar carbon concentrations but reversed B:N molar ratios, we observe that the type of band gap remains the same. $B_{13}C_8N_{11}$ and $N_{13}C_8B_{11}$ have metallic band gaps, whereas $B_{11}C_{12}N_9$ and $N_{11}C_{12}B_9$ have indirect band gaps.

C_2-doped-4×4-BN and C_4-doped-4×4-BN have direct band gaps of 3.37 and 2.71 eV, respectively (Table 2 and Fig. 2(b) and 2(c)). The decrease in band gap between C_2-doped-4×4-BN and C_4-doped-4×4-BN indicates an inverse relationship between the C atom concentration and band gap. This trend matches the findings of Huang et al., who showed that the BN band gap can be

Table 2. Calculated band gaps for all monolayers in the present study.

Monolayer	Band gap (eV)	Band gap type
4×4-BN	4.27	Indirect
N_v-4×4-BN	1.35	Indirect
C_2-doped 4×4-BN	3.37	Direct
C_4-doped 4×4-BN	2.71	Direct
$B_{13}C_8N_{11}$	0	Metallic
O_C-$B_{13}C_8N_{11}$	1.90	Indirect
O_N-$B_{13}C_8N_{11}$	2.44	Direct
$N_{13}C_8B_{11}$	0	Metallic
$B_{11}C_{12}N_9$	0.03	Indirect
$N_{11}C_{12}B_9$	0.25	Indirect
2×2-BC_6N	1.27	Direct
O_C-2×2-BC_6N	0.23	Indirect
O_N-2×2-BC_6N	0	Metallic
Si_C-2×2-BC_6N	0.90	Direct

(a) N_v-4x4-BN

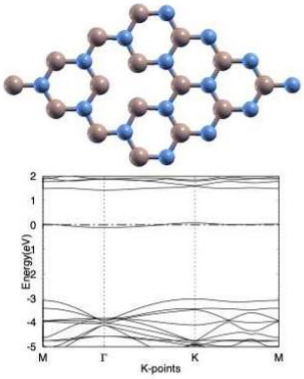

(b) C_2-4x4-BN

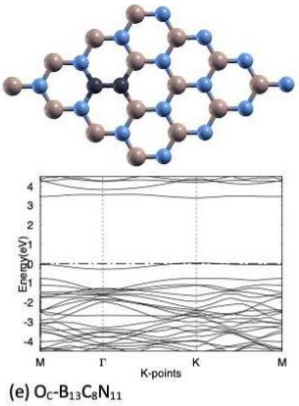

(c) C_4-4x4-BN

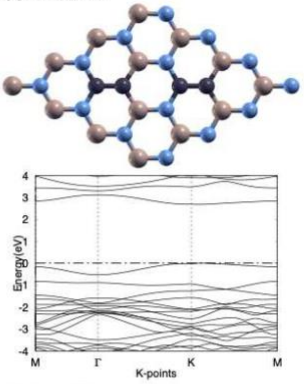

(d) $B_{13}C_8N_{11}$

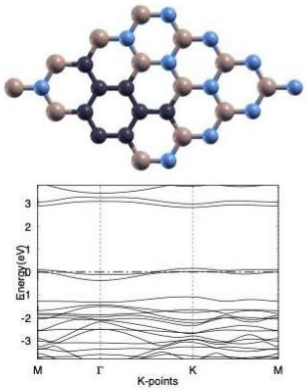

(e) O_C-$B_{13}C_8N_{11}$

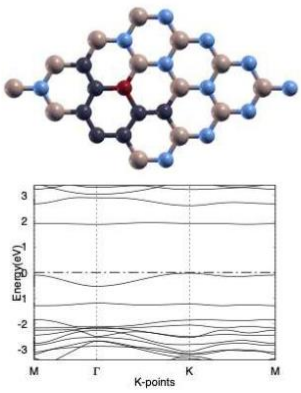

(f) O_N-$B_{13}C_8N_{11}$

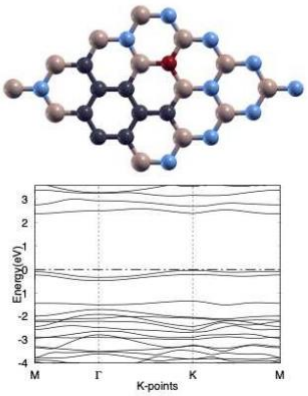

(g) $N_{13}C_8B_{11}$

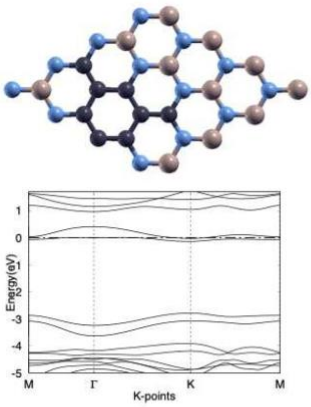

(h) $B_{11}C_{12}N_9$

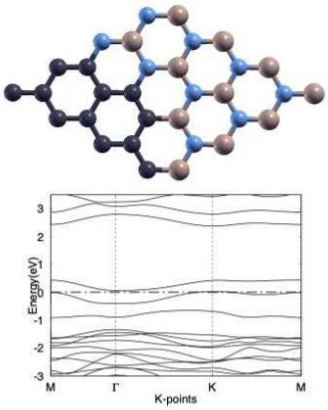

(i) $N_{11}C_{12}B_9$

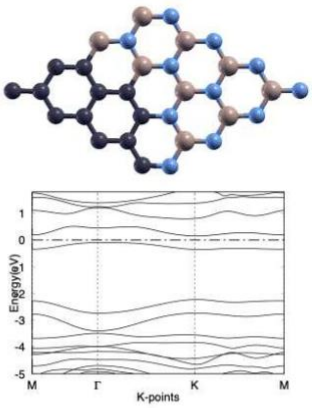

(j) O_C-2x2-BC_6N

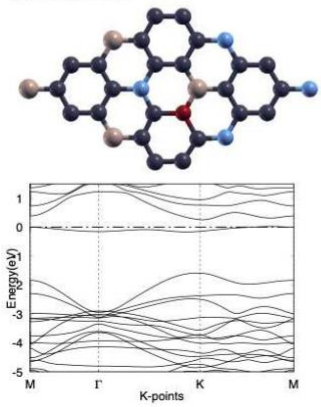

(k) O_N-2x2-BC_6N

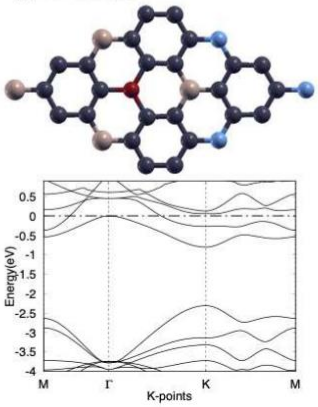

(l) Si_C-2x2-BC_6N

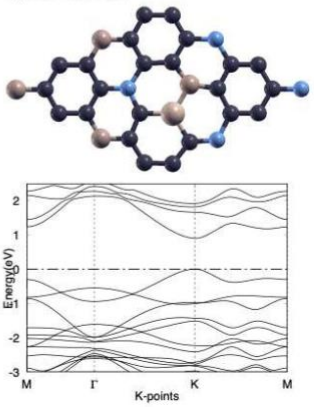

Fig. 2. Relaxed atomic and band structure plots of the studied monolayers: (a) N_V-4×4-BN, (b) C_2-4×4-BN, (c) C_4-4×4-BN, (d) $B_{13}C_8N_{11}$, (e) O_C-$B_{13}C_8N_{11}$, (f) O_N-$B_{13}C_8N_{11}$, (g) $N_{13}C_8B_{11}$, (h) $B_{11}C_{12}N_9$, (i) $N_{11}C_{12}B_9$, (j) O_C-2×2-BC_6N, (k) O_N-2×2-BC_6N, and (l) Si_C-2×2-BC_6N.

tuned for specific functions by varying the C atom concentration.[26] This finding motivated us to further modify the materials by varying their C atom concentrations. We note that the band structures of the two monolayers ($B_{13}C_8N_{11}$ and $B_{11}C_{12}N_9$) were misinterpreted by Huang et al. Specifically, the band gaps determined in their study were large defect levels instead of direct band gaps. Therefore, these structures are incapable of CO_2 photo-redox catalysis, as previously proposed.

CO_2 and monolayer complexes

Another important aspect of CO_2 catalysis is the adsorption of CO_2 on the monolayer. CO_2 chemisorption ($E_{ad} \leq -0.3$ eV) is necessary for the reduction reaction to occur. We calculated the E_{ad} of CO_2 on monolayers with a suitable band gap for photocatalysis and monolayers we expected to have good CO_2 adsorption properties. The E_{ad}, adsorption type, and gas–monolayer distance (d) of these monolayers are summarized in Table 3. According to the results shown, modification of the pristine BN and BCN monolayers renders surface CO_2 adsorption more energetically favorable. The unmodified 4×4-BN and 2×2-BC_6N monolayers have positive CO_2 E_{ad} values, indicating that CO_2 cannot spontaneously adsorb onto these monolayers. These positive E_{ad} values are in good agreement with previous studies of these two materials, which indicates that modification of these materials to facilitate adsorption could be a worthwhile strategy.[30,40]

The rest of the relaxed monolayers demonstrated adsorption (i.e., $E_{ad} < 0$) to CO_2. Their relaxed structures are shown in Fig. 3, and Table 4 lists the band gap values and types of these complex structures. Unmodified $B_{13}C_8N_{11}$ and $B_{11}C_{12}N_9$ demonstrate low E_{ad} values of −0.037 and −0.007 eV, respectively. Thus, both monolayers can only physically adsorb CO_2, indicating that London

Table 3. CO_2 adsorption energy E_{ad}, adsorption type, and gas–monolayer distance (d) of selected monolayers.

Complex configuration	E_{ad} (eV)	Adsorption type	d (Å)
4×4-BN	0.004	No adsorption	3.71
N_v-4×4-BN	−3.881	Chemisorption	0.00
$B_{13}C_8N_{11}$	−0.037	Physisorption	4.42
O_N-$B_{13}C_8N_{11}$ (CO detached)	−1.870	Chemisorption	1.22
O_N-$B_{13}C_8N_{11}$ (CO_2 adsorbed)	−0.041	Physisorption	4.20
$B_{11}C_{12}N_9$	−0.007	Physisorption	6.51
2×2-BC_6N	0.061	No adsorption	3.21
O_C-2×2-BC_6N	−1.801	Chemisorption	1.44
Si_C-2×2-BC_6N	−1.480	Chemisorption	3.51

dispersion forces may be the dominant interactions. Because physisorbent materials tend to show low selectivity for CO_2, they are unsuitable for carbon capture.

To study in more detail for the O_N-$B_{13}C_8N_{11}$ monolayer that demonstrated strong adsorption, we investigated two CO_2 adsorption locations. Placing CO_2 closer to the hexagonal center leads to a strong attraction between the O atom and the C and B atoms (E_{ad} = -1.870 eV), forming chemical bonds to the monolayer. This interaction yields a CO molecule that is only slightly attracted to the monolayer, indicating that CO_2 was reduced to CO.

Next, we placed CO_2 farther from the monolayer in the vertical direction to study whether the entire molecule can be chemisorbed on the monolayer without reduction and, hence, serve as a CO_2 capture material. In this case, CO_2 exhibits only a weak physisorption of −0.041 eV with the monolayer after relaxation, meaning that reduction is more energetically favorable than adsorption given the ideal initial position. Among all selected monolayers, O_N-$B_{13}C_8N_{11}$ (CO

detached), O_C-2×2-BC_6N, Si_C-2×2-BC_6N, and N_v-4×4-BN demonstrate chemisorption for CO_2, with $E_{ad} \leq -0.3$ eV.

Therefore, charge transfer in these cases demonstrating chemisorption was plotted using Eq. (1) to observe the change in electron density distribution caused by interactions between CO_2 and the monolayers. As shown in Fig. 4, the pink and green regions represent charge accumulation and charge depletion, respectively. Charge is transferred from the green regions to the pink regions.

For O_N-$B_{13}C_8N_{11}$ with detached CO, as shown in Fig. 4(a), electrons were transferred from the O_N-$B_{13}C_8N_{11}$ monolayer to the chemically bonded O atom. The charge accumulates in the region of newly formed B–O and C–O bonds, which cover the O atom, indicating strong chemisorption between the O atom and the monolayer. The CO molecule is located far from the monolayer, meaning that it exhibits a low attraction to the monolayer. This finding is consistent with the E_{ad} calculations and confirms strong chemisorption between the O atom and the monolayer.

For N_v-4×4-BN, shown in Fig. 4(b), there is considerable charge accumulation on the attached O atom of CO_2, rendering the surrounding B atoms electron deficient. This observation is in accordance with the difference in electronegativity between B and O and confirms

Table 4. Band gaps of CO_2 adsorbed on selected monolayers.

Selected monolayer	Band gap (eV)	Band gap type
N_v-4×4-BN	0.87	Indirect
$B_{13}C_8N_{11}$	0	Metallic
O_N-$B_{13}C_8N_{11}$ (CO detached)	2.42	Direct
O_N-$B_{13}C_8N_{11}$ (CO_2 adsorbed)	2.44	Direct
$B_{11}C_{12}N_9$	0.04	Indirect
O_C-2×2-BC_6N	1.06	Indirect
Si_C-2×2-BC_6N	1.33	Indirect

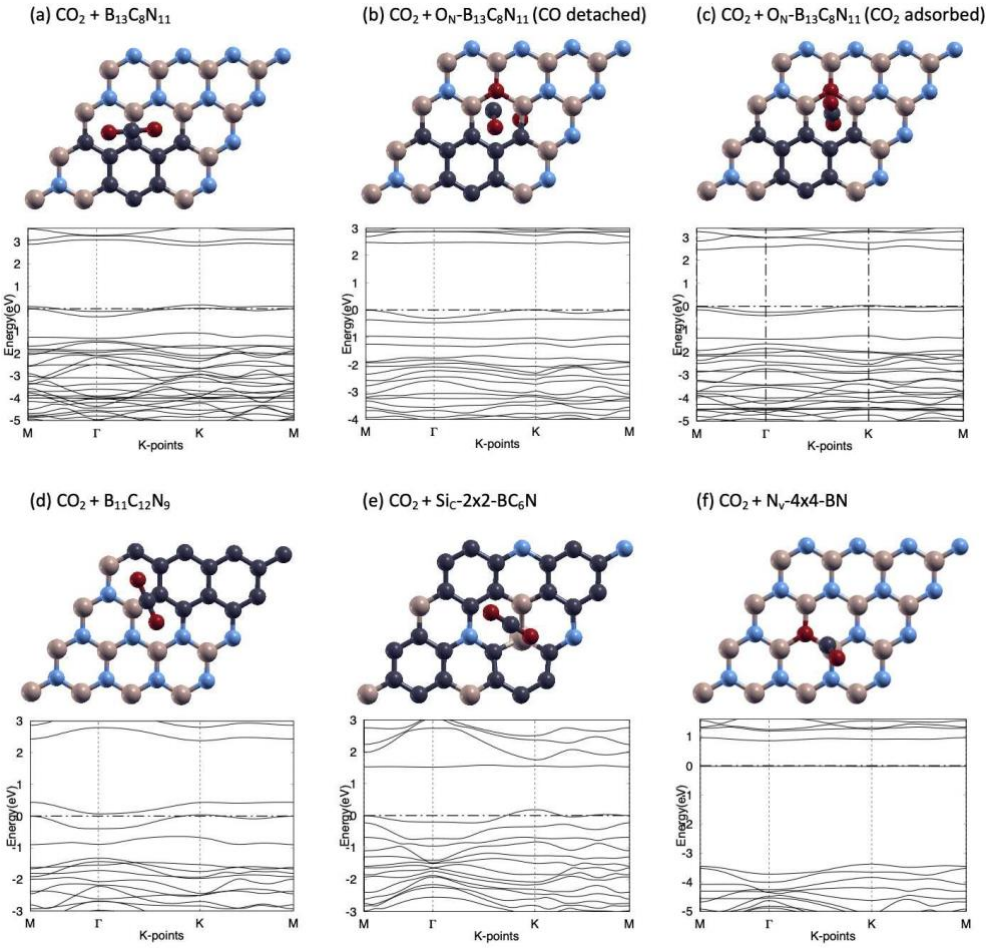

Fig. 3. Relaxed atomic and band structure plots of (a) $B_{13}C_8N_{11}$ with top-adsorbed CO_2, (b) O_N-$B_{13}C_8N_{11}$ with detached CO, (c) O_N-$B_{13}C_8N_{11}$ with adsorbed CO_2, (d) $B_{11}C_{12}N_9$ with top-adsorbed CO_2, (e) Si_C-2×2-BC_6N with top-adsorbed CO_2, and (f) N_v-4×4-BN with CO_2 adsorbed in site of vacancy. The Fermi level was set to 0 eV. B and Si atoms are shown in pink, C atoms are shown in black, N atoms are shown in blue, and O atoms are shown in red.

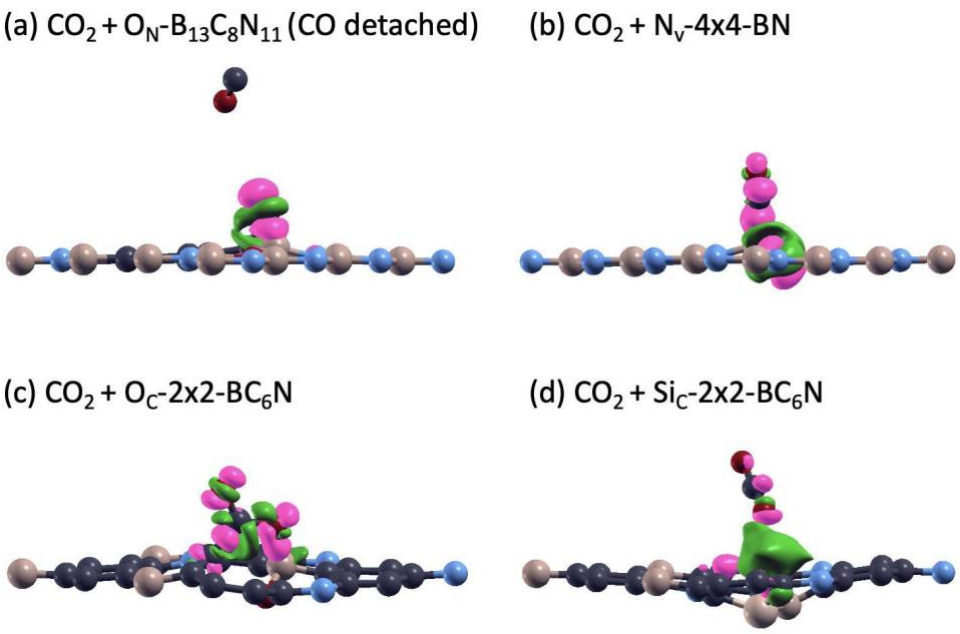

Fig. 4. Charge transfer between CO_2 and selected monolayers that demonstrated chemisorption with CO_2. (a) O_N-$B_{13}C_8N_{11}$ with detached CO (isovalue = 6.75 × 10^{-2} electron/Å^3), (b) N_v-4×4-BN (isovalue = 6.75 × 10^{-2} electron/Å^3), (c) O_C-2×2-BC_6N (isovalue = 6.75 × 10^{-2} electron/Å^3), and (d) Si_C-2×2-BC_6N (isovalue = 1.35 × 10^{-3} electron/Å^3). B and Si atoms are shown in pink, C atoms are shown in black, N atoms are shown in blue, and O atoms are shown in red.

the chemical interaction between the bonded CO_2 gas and the N_v-4×4-BN monolayer.

For O_C-2×2-BC_6N and Si_C-2×2-BC_6N, as shown in Fig. 4(c) and 4(d), O atoms tend to attract more charge than the other elements because of their high electronegativity. Thus, charge density accumulates more at the O atom that is closer to the monolayer, leaving the corresponding monolayer region electron deficient.

Therefore, the charge transfers confirm the chemisorption between the monolayers and CO_2 and provides insights into the CO_2 reduction process.

Applications

Considering both the bandgap and E_{ad} of the monolayers, O_N-$B_{13}C_8N_{11}$ and Si_C-2×2-BC_6N are suitable potential CO_2 reduction photocatalysts, adding to the relatively less explored non-metallic photocatalysts. The reduction potential of O_N-$B_{13}C_8N_{11}$ is suggested by the dissociation of the C–O bond in CO_2 during adsorption. However, bond dissociation occurs in the absence of visible light, indicating that this type of catalysis may not be a photodriven process. Nonetheless, the detached

CO can be further utilized. While the electrochemical conversion of CO_2 into single-carbon products can be controlled relatively easily, its direct conversion into C_{2+} products is more environmentally friendly and commercially favorable.[41] As the direct conversion of CO_2 into C_{2+} products currently suffers from unwanted side reactions and relatively low selectivity, this conversion can be achieved more effectively with CO as the key reaction intermediate.[42] Studies on electrochemical CO reduction demonstrate promising potential for producing vital short-chain C_{2+} products, including ethylene, ethanol, acetic acid, and *n*-propanol, etc., which can be converted into plastics, fuels, and feedstocks.

Although the other studied monolayers cannot serve as CO_2 photocatalysts, their band structures and adsorption abilities allow them to be used in other applications. For instance, the strong CO_2 chemisorption exhibited by O_C-2×2-BC_6N and N_v-4×4-BN renders them good CO_2 capture materials. Monolayers with metallic characteristics and demonstrating CO_2 physisorption, such as $B_{13}C_8N_{11}$, can be further developed into charge-regulated materials for CO_2 capture, as their properties are similar to those of other charge-regulated CO_2 capture materials. [43]

Many of these complex materials exhibited indirect band gaps after interacting with CO_2, as seen in Table 4. Notably, the change in band gap will not hinder their previously discussed visible-light absorption properties, as the influence of CO_2 adsorption on the global band gap increases because CO_2 is arranged in a periodic manner in the conducted calculations. In reality, the concentration of CO_2 molecules adsorbed on these materials is much lower than that used in calculations, inducing a local change in the band structure rather than a global change. Therefore, the band gaps of these monolayers are indicative of their visible-light adsorption ability.

The band structures of the selected monolayer complexes will be valuable for further studies. For instance, the 2.44 eV direct band gap of O_N-$B_{13}C_8N_{11}$ (with adsorbed CO_2) can be useful in fabricating optical devices, such as LEDs and semiconductor lasers. Complexes with small indirect band gaps may have potential in optoelectronic thin-film technologies.[44]

Although out research outlined the potential applications of the selected monolayers in these fields, further systematic theoretical studies should be implemented to determine the most ideal structural design for practical applications. Also, the specific placement of CO_2 on the monolayers used in this research might restrict the applicability of the materials when CO_2 is not positioned ideally, suggesting further investigation.

Conclusion

In conclusion, we used DFT calculations to investigate the atomic and electronic structures of BN- and BCN-based monolayers as well as their interactions with CO_2 gas. By modifying the structural configuration of the monolayers through doping and vacancy creation methods, we successfully tuned the band gaps of these monolayers and improved the adsorption of CO_2. The calculated results indicated that O_N-$B_{13}C_8N_{11}$ and Si_C-2×2-BC_6N are suitable CO_2 photocatalysts, whereas O_C-2×2-BC_6N and N_v-4×4-BN are capable of CO_2 capture. Other monolayers capable of CO_2 adsorption possessed favorable properties for utilization in optoelectronic materials. In summary, the novel metal-free materials proposed in this research lays a strong theoretical basis that facilitates the development of existing CCU approaches and is inspiring for prospective work in this field.

As doping with O and Si atoms can increase the monolayers' attraction from no attraction or physisorption to chemisorption for CO_2, future studies could explore the impact of other non-metallic dopants or the concentration of dopants on the materials' electronic structure and interaction with CO_2. The effect of layer thickness on CO_2 photoreduction can also be further investigated as the current research only focused on monolayer materials. Projected density of states (PDOS) calculations will also be helpful in studying the more detailed mechanism of the interaction between the monolayer and CO_2.

References

[1] WMO. Global temperatures set to reach new records in next five years, May 2023.

[2] Paritosh Kasotia. The health effects of global warming: Developing countries are the most vulnerable.

[3] WHO. Climate change and health, Oct 2021.

[4] Zhenyu Sun, Neetu Talreja, Hengcong Tao, John Texter, Martin Muhler, Jennifer Strunk, and Jianfeng Chen. Nanosheet catalysis of carbon dioxide photoreduction on nanosheets: Fundamentals and challenges. *Angewandte Chemie International Edition*, 57(26):7610–7627, Jun 2018.

[5] Rebecca Lindsey. Climate change: Atmospheric carbon dioxide—noaa climate.gov, May 2023.

[6] Ahmed Al-Mamoori, Anirudh Krishnamurthy, Ali A. Rownaghi, and Fateme Rezaei. Carbon capture and utilization update. *Energy Technology*, 5(6):834–849, Jun 2017.

[7] Matthew E.Boot-Handford, Juan C.Abanades, Edward J.Anthony, Martin J.Blunt, Stefano Brandani, Niall Mac Dowell, J Fernandez, Maria-Chiara Ferrari, Robert Gross, Jason P.Hallett, R. Stuart Haszeldine, Philip Heptonstall, Anders Lyngfelt, Zen Makuch, Enzo Mangano, Richard T. J. Porter, Mohamed Pourkashanian, Gary T. Rochelle, Nilay Shah, Joseph G. Yao, and Paul S. Fennell. Carbon capture and storage update. *Energy Envir Sci*, 7(1):130–189, 2014.

[8] Chi Chen, Juliet F. Khosrowabadi Kotyk, and Stafford W. Sheehan. Progress toward commercial application of electrochemical carbon dioxide reduction. *Chem*, 4(11):2571–2586, Nov 2018.

[9] Nomie Elgrishi, Matthew B. Chambers, Xia Wang, and Marc Fontecave. Molecular polypyridine-based metal complexes as catalysts for the reduction of co2. *Chemical Society Reviews*, 46(3):761–796, Feb 2017.

[10] James L. White, Maor F. Baruch, James E. Pander, Yuan Hu, Ivy C. Fortmeyer, James Eujin Park, Tao Zhang, Kuo Liao, Jing Gu, Yong Yan, Travis W. Shaw, Esta Abelev, and Andrew B. Bocarsly. Light-driven heterogeneous reduction of carbon dioxide: Photocatalysts and photoelectrodes. *Chemical Reviews*, 115(23):12888–12935, Dec 2015.

[11] Xin Li, Jiaguo Yu, Mietek Jaroniec, and Xiaobo Chen. Cocatalysts for selective photoreduction of co2 into solar fuels. *Chemical Reviews*, 119(6):3962–4179, Mar 2019.

[12] Bhawna, Sanjeev Kumar, Ritika Sharma, Shikha Jyoti Borah, Akanksha Gupta, Manoj Kumar Gupta, Ravinder Kumar, Kashyap Kumar Dubey, Yogendra Kumar Mishra, and Vinod Kumar. Catalytic heterostructured materials for co2 mitigation and conversion into fuels: a renewable energy approach towards a sustainable environment. *Sustainable Energy Fuels*, 4354-4359, Jul 2023.

[13] Milad Laghaei, Mohsen Ghasemian, Weiwei Lei, Lingxue Kong, and Qi Chao. A review of boron nitride-based photocatalysts for carbon dioxide reduction. *Journal of Materials Chemistry A*, 11(23):11925–11963, 2023.

[14] Yan Cui, Pengxiang Ge, Mindong Chen, and Leilei Xu. Research progress in semiconductor materials with application in the photocatalytic reduction of co2. *Catalysts*, 12(4):372, Mar 2022.

[15] Ji Yong Choi, Chan Kyu Lim, Bumjin Park, Minjun Kim, Aqil Jamal, and Hyunjoon Song. Surface activation of cobalt oxide nanoparticles for photocatalytic carbon dioxide reduction to methane. *Journal of Materials Chemistry A*, 7(25):15068–15072, Jun 2019.

[16] Bingbing Hu, Maocong Hu, Qiang Guo, Kang Wang, and Xitao Wang. In-vacancy engineered plate-like in(oh)3 for effective photocatalytic reduction of co2 with h2o vapor. *Applied Catalysis B: Environmental*, 253:77–87, Sep 2019.

[17] Huidong Shen, Tim Peppel, Jennifer Strunk, and Zhenyu Sun. Photocatalytic reduction of co2 by metal-free-based materials: Recent advances and future perspective. *Solar RRL*, 4(8), 2020.

[18] Yansong Zhou, Zhitong Wang, Lei Huang, Shahid Zaman, Kai Lei, Ting Yue, Zhong'an Li, Bo You, and Bao Yu Xia. Engineering 2d photocatalysts toward carbon dioxide reduction. *Advanced Energy Materials*, 11(8):2003159, Feb 2021.

[19] Jingshuai Chen, Feng Xin, Helin Niu, Chang-Jie Mao, and Ji-Ming Song. Photocatalytic reduction of co2 with methanol over bi2s3-znin2s4 nanocomposites. *Materials Letters*, 198:1–3, Jul 2017.

[20] Pawan Kumar, Harshal P. Mungse, Om P. Khatri, and Suman L. Jain. Nitrogen-doped graphene-supported copper complex: a novel photocatalyst for co2 reduction under visible light irradiation. *RSC Advances*, 5(68):54929–54935, Jun 2015.

[21] Xin Li, Jiaguo Yu, and Mietek Jaroniec. Hierarchical photocatalysts. *Chemical Society Reviews*, 45(9):2603–2636, May 2016.

[22] Kohsuke Mori, Hiromi Yamashita, and Masakazu Anpo. Photocatalytic reduction of co 2 with h2o on various titanium oxide photocatalysts. *RSC Advances*, 2(8):3165–3172, 2012.

[23] Zhiyong Wang, Yuan Pu, Dan Wang, Jie-Xin Wang, and Jian-Feng Chen. Recent advances on metal-free graphene-based catalysts for the production of industrial chemicals. *Frontiers of Chemical Science and Engineering*, 12(4):855–866, Dec 2018.

[24] Fangshu Xing, Qiuwen Liu, Mingxia Song, and Caijin Huang. Fluorine modified boron carbon nitride semiconductors for improved photocatalytic co 2 reduction under visible light. *ChemCatChem*, 10(22):5270–5279, Nov 2018.

[25] Lutfi Kurnianditia Putri, Wee-Jun Ong, Wei Sea Chang, and Siang-Piao Chai. Heteroatom doped graphene in photocatalysis: A review. *Applied Surface Science*, 358:2–14, Dec 2015.

[26] Caijin Huang, Cheng Chen, Mingwen Zhang, Lihua Lin, Xinxin Ye, Sen Lin, Markus Antonietti, and Xinchen Wang. Carbon-doped bn nanosheets for metal-free photoredox catalysis. *Nature Communications*, 6(11):7698, Jul 2015.

[27] Bin Huang, Yifan Wu, Yaorong Luo, and Naigen Zhou. Double atom-anchored defective boron nitride catalyst for efficient electroreduction of co2 to ch4: A first principles study. *Chemical Physics Letters*, 756, 137852, Oct 2020.

[28] Manjot Kaur, Kulwinder Singh, Ankush Vij, and Akshay Kumar. Recent insights into bcn nanomaterials – synthesis, properties and applications. *New Journal of Chemistry*, 47(5):2137–2160, 2023.

[29] Abhishek Kumar Mishra and Soni Mishra. Tuning of adsorption energies of co2 and ch4 in borocarbonitrides bxcynz: A first-principles study. *Journal of Molecular Graphics and Modelling*, 93:107446, Dec 2019.

[30] A. Bafekry. Graphene-like bc6n single-layer: Tunable electronic and magnetic properties via thickness, gating, topological defects, and adatom/molecule. *Physica E: Low-dimensional Systems and Nanostructures*, 118:113850, Apr 2020.

[31] Jiahui Yu, Chaozheng He, Chunying Pu, Ling Fu, Dawei Zhou, Kun Xie, Jinrong Huo, Chenxu Zhao, and Lingmin Yu. Prediction of stable bc3n2 monolayer from first-principles calculations: Stoichiometry, crystal structure, electronic and adsorption properties. *Chinese Chemical Letters*, 32(10):3149–3154, Oct 2021.

[32] Yuehan Cao, Ruiyang Zhang, Tianli Zhou, Shengming Jin, Jindi Huang, Liqun Ye, Zeai Huang, Fang Wang, and Ying Zhou. B-o bonds in ultrathin boron nitride nanosheets to promote photocatalytic carbon dioxide conversion. *ACS Appl. Mater. Interfaces*, 12(8):9935–9943, Feb 2020.

[33] Sherif Abdulkader Tawfik, X. Y. Cui, S. P. Ringer, and C. Stampfl. Multiple co 2 capture in stable metal-doped graphene: a theoretical trend study. *RSC Advances*, 5(63):50975–50982, 2015.

[34] X. Gonze, B. Amadon, P.-M. Anglade, J.-M. Beuken, F. Bottin, P. Boulanger, F. Bruneval, D. Caliste, R. Caracas, M. Cote, T. Deutsch, L. Genovese, Ph. Ghosez, M. Giantomassi, S. Goedecker, D.R. Hamann, P. Hermet, F. Jollet, G. Jomard, S. Leroux, M. Mancini, S. Mazevet, M.J.T. Oliveira, G. Onida, Y. Pouillon, T. Rangel, G.-M. Rignanese, D. Sangalli, R. Shaltaf, M. Torrent, M.J. Verstraete, G. Zerah,

and Zwanziger. Abinit: First-principles approach of materials and nanosystem properties. *Computer Physics Communications*, 180:2582– 2615, 2009.

[35] P.E. Blochl. Projector augmented-wave method. *Phys. Rev. B*, 50(24):17953–17979, Dec 1994.

[36] N. A. W. Holzwarth, A. R. Tackett, and G. E. Matthews. A projector augmented wave (paw) code for electronic structure calculations, part i: atompaw for generating atom-centered functions. *Computer Physics Communications*, 135:329–347, 2001.

[37] George Glockler. Carbon-oxygen bond energies and bond distances. *The Journal of Physical Chemistry*, 62(9):1049–1054, Sep 1958.

[38] Geunsik Lim, Ki Bong Lee, and Hyung Chul Ham. Effect of n-containing functional groups on co 2 adsorption of carbonaceous materials: A density functional theory approach. *The Journal of Physical Chemistry C*, 120(15):8087–8095, Apr 2016.

[39] Oleksandr O. Kurakevych and Vladimir L. Solozhenko. Rhombohedral boron subnitride, b13n2, by x-ray powder diffraction. *Acta Crystallographica. Section C, Crystal Structure Communications*, 63(Pt 9):80–82, Sep 2007.

[40] Jiahui Yu, Chaozheng He, Jinrong Huo, Chenxu Zhao, and Lingmin Yu. Electric field controlled co2 capture and activation on bc6n monolayers: A first-principles study. *Surfaces and Interfaces*, 30:101885, Jun 2022.

[41] Phil De Luna, Christopher Hahn, Drew Higgins, Shaffiq A. Jaffer, Thomas F. Jaramillo, and Edward H. Sargent. What would it take for renewably powered electrosynthesis to displace petrochemical processes? *Science*, 364(6438), Apr 2019.

[42] Matthew Jouny, Gregory S. Hutchings, and Feng Jiao. Carbon monoxide electroreduction as an emerging platform for carbon utilization. *Nature Catalysis*, 2(12):1062–1070, Dec 2019.

[43] Haihui Zhang, Huihui Xiong, and Wei Liu. Sic3 as a charge-regulated material for co2 capture. *Crystals*, 11(55):543, May 2021.

[44] Jiban Kangsabanik, Mark Kamper Svendsen, Alireza Taghizadeh, Andrea Crovetto, and Kristian S. Thygesen. Indirect band gap semiconductors for thin-film photovoltaics: High-throughput calculation of phonon-assisted absorption. *Journal of the American Chemical Society*, 144(43):19872–19883, Nov 2022.

Acknowledgments

This work is inspired by the unique potentials of BCN monolayer materials that can have different designs and be modified through doping and vacancy creation. Under the context of global warming and climate change and following the green chemistry concept, the metal-free modification approach is used, and the monolayers' application in CO_2 capture and utilization was devised.

Jingyuan Wang conceived and designed the research procedures, carried out DFT calculations, visualized data, and contributed to writing the original draft, reviewing, and editing the draft. Dr. Xuan Luo helped in designing the methodology and writing – reviewing and editing. All of her help is non-profit.

The author would like to sincerely thank Dr. Xuan Luo for her guidance and advice in this research. I gained much knowledge and experience in this field of chemistry through this research.